Nano Research 2018, 11(1): 174–184
https://doi.org/10.1007/s12274-017-1617-0
Research Article
ISSN 1998-0124
CN 11-5974/O4

Graphene quantum dots derived from hollow carbon nano-onions

Chenguang Zhang[1,3], Jiajun Li[2], Xianshun Zeng[1], Zhihao Yuan[1,3] (✉), and Naiqin Zhao[2,4] (✉)

[1] *School of Materials Science and Engineering, Tianjin University of Technology, Tianjin 300384, China*
[2] *School of Materials Science and Engineering, Tianjin University, Tianjin 300072, China*
[3] *Tianjin Key Lab for Photoelectric Materials & Devices, Tianjin 300384, China*
[4] *Collaborative Innovation Center of Chemical Science and Engineering, Tianjin University, Tianjin 300072, China*

Received: 30 January 2017
Revised: 6 April 2017
Accepted: 9 April 2017

KEYWORDS
graphene quantum dots, carbon nano-onions, fluorescent quenching, bioimaging

ABSTRACT

Herein, carbon nano-onions (CNOs) with different structures have been investigated as precursors for the synthesis of graphene quantum dots (GQDs). It was found that hollow CNOs yield GQDs with a uniform size distribution, whereas metal encapsulation in the CNO structure is disadvantageous for the same. Furthermore, the hollow CNOs are also advantageous for the synthesis of GQDs with a yellow-green hybrid luminescence and long-ranged excitation wavelength (λ_{ex})-independent photoluminescent (PL) behavior, in which the λ_{ex} upper limit was 480 nm. These features enable safe sensing and cell tracking applications with a longer excitation wavelength in the visible light region. The potential applications of the synthesized GQDs as fluorescent sensing probes for detecting Cu(II) ions and non-toxic cell imaging under visible light excitation have been demonstrated. This means that sensing and bioimaging can be accomplished in the natural environment with no need for UV excitation. This work provides a reference to researchers in tailoring CNO structures in terms of their inner space to synthesize GQDs with the desired luminescence behavior.

1 Introduction

Graphene quantum dots (GQDs) have been drawing much attention due to their intrinsic non-toxicity making them an alternative to the conventional semiconducting quantum dots in sensing and biological applications. The photoluminescence originating from the quantum confinement and edge effects makes them new-generation fluorescent probes [1–3]. Tunable photoluminescence can be realized by varying the surface functionalization state [2, 4], sizes of the quantum dots [5] and conjugated sp^2-domains [6], nitrogen doping amount [7] and nitrogen functionalization groups [8]. However, most GQDs or carbon quantum dots exhibit the main photoluminescence peak wavelength (λ_{PL}) in the short λ region below 500 nm [9–14] or an excitation wavelength (λ_{ex}) highly dependent behavior if their λ_{PL} is above 450 nm

Address correspondence to Zhihao Yuan, zhyuan@tjut.edu.cn; Naiqin Zhao, nqzhao@tju.edu.cn

[10, 11, 13, 15, 16]. Although some GQDs are able to show a low λ_{ex}-dependent PL behavior when their λ_{PL} is above 500 nm, the upper limit of λ_{ex} for this behavior was only 440 nm [3] and it was found that the λ_{ex} region for this PL behavior is narrow [17]. For safe and efficient cell imaging under visible light excitation with no UV light, GQDs with a longer λ_{PL} in the visible region and λ_{ex}-independent PL behavior in a wide λ_{ex} range with a high λ_{ex} upper limit are required.

Precursors play an important role in determining the PL behavior of the GQDs. Typically, graphene quantum dots are graphene fragments less than 10 nm in size, with a sp^2-carbon framework and surfaces coated with oxygen-containing groups [2], polymers, or other species. Therefore, it would be ideal to produce GQDs from precursors containing small sp^2-carbon domain structures. To this end, different precursors have been employed to synthesize GQDs, including graphene, carbon black [18], carbon fibers [19], and coal [10, 20]. The precursor structure and atomic arrangement have a great influence on the structure and PL behavior of the resultant GQDs. Tour and co-workers [20] demonstrated that the GQDs derived from bituminous coal have a smaller size and a uniform size distribution than those derived from coke and anthracite. Qiu and co-workers [10] found that coal treated at high carbonization temperatures yielded large GQDs with a red-shift PL as compared to that treated at lower temperatures or without treatment. Lin et al. [7] demonstrated that different phenylenediamine isomers yield GQDs with different luminescence properties. Carbon nano-onions (CNOs) are sp^2-carbon structured nanocarbon allotropes, with spherical closed graphitic shells a few nanometers thick. The CNOs usually have curved non-closed shells and structural defects such as holes within the sp^2-shells [21]. Besides, the highly curved surfaces in the nanometer size range have a high surface energy. Thus, CNOs are expected to be the perfect precursors to be exfoliated into smaller-sized GQDs. C_{60}, which is considered as the innermost single carbon shell of the onion-like carbon structures, has been transformed into GQDs using a Ru substrate [22]. Recently, Kim and co-workers demonstrated the possibility of using CNOs as the precursors for the synthesis of ultraviolet and blue emissive GQDs [11]. However, the influence of the CNO structures on the synthesis of GQDs has not yet been studied. Previous studies inspired us to tailor the CNO precursor structures to obtain GQDs with the desired size, size distribution, and PL behavior.

Herein, two typical types of CNOs were employed to synthesize GQDs by acid oxidation; among various top-down methods for producing GQDs, acid oxidation has been found to be very facile and advantageous [7, 9, 23, 24]. We demonstrate that hollow CNOs are the preferential candidate precursors for the synthesis of GQDs with a uniform size distribution, whereas the metal encapsulating CNOs are disadvantageous for the same. Furthermore, the hollow CNOs are also favorable for the synthesis of GQDs with a yellow-green hybrid luminescence over a broad excitation wavelength spectrum and a λ_{ex}-independent PL behavior, in which the maximum λ_{ex} was 480 nm, which is much higher than the wavelength previously reported [10, 11, 13, 15, 16]. These characteristics enable sensing and cell tracking applications with longer λ_{ex} excitation in the visible region. The influence of the CNO structure on the structure and PL behavior of the resultant GQDs was investigated and a mechanism has been proposed to explain the same. Finally, the potential applications of the synthesized GQDs as fluorescent sensing probes for detecting Cu(II) ions and in non-toxic cell imaging using visible light excitation have been demonstrated. This work will provide a reference to researchers in tailoring the CNO structure, in terms of the inner space, to synthesize GQDs with the desired PL behavior.

2 Experimental

2.1 Synthesis of GQDs

Two types of hollow CNOs were employed for synthesizing the GQDs. The first type were prepared by high temperature annealing of metal encapsulating CNOs, according to our previous report [25], and the second type were commercially obtained from the Institute of Solid State Physics, Chinese Academy of Sciences. The metal (Fe, Ni, and Fe-Ni alloy) encapsulating CNOs were prepared according to the procedure we reported earlier [26, 27]. The processes for the synthesis of high temperature annealing derived

hollow CNOs and metal encapsulating CNOs are described in the supporting information. The GQDs were prepared by chemically oxidizing the hollow CNOs or metal encapsulating CNOs in a mixture of H_2SO_4 (18.4 M) and HNO_3 (14.4 M) (60/20 v/v). Briefly, 200 mg of the CNOs was dispersed in 80 mL of the H_2SO_4 and HNO_3 solution and subjected to ultrasonication for 0.5 h to acidify the CNOs and make them soluble. Later, the CNO containing solution was heated to 100 ˚C in an oil bath and refluxed for 5 h. The solution was cooled down to room temperature, and NaOH pills were added to neutralize the strong acid solution. The addition of pills was carried out until the pills were no longer soluble. The neutralized solution was then heated in a rotary evaporator to shrink reduce the volume for carrying out dialysis. Dialysis was conducted overnight until the dialyzed-out solution was neutralized and showed no precipitation when tested with $BaCl_2$ solution to ensure complete removal of the residual metal ions. The GQDs were obtained by freeze-drying the purified solution. For subsequent testing, the lyophilized product was re-dissolved in deionized water to prepare the GQD solutions at the required concentrations.

2.2 Characterizations

Transmission electron microscopy (TEM) and high-resolution transmission electron microscopy (HRTEM) characterizations were conducted on a JEOL 2100F field emission gun TEM at 200 kV. Atomic force microscopy (AFM) images were obtained on a Digital Instrument Nanoscope IIIA. Raman spectra were generated on a Renishaw inVia Raman spectrometer using an Ar^+ laser with an excitation wavelength of 514 nm. X-ray photoelectron spectroscopy (XPS) measurements were performed on a VG ESCALAB 220i-XL system using a monochromatic Al Kα source (1,486.6 eV). UV–Vis spectra were recorded using a 2501PC UV-Vis spectrophotometer. Fluorescence spectra of the GQDs were analyzed using a RF-5301 fluorescence spectrometer. Fourier transform infrared (FTIR) spectra were recorded on a FTS6000 FTIR microscope. Time-resolved photoluminescence spectra were generated using a FLSP-920 Edinburgh-spectrometer, equipped with 370 nm picosecond laser diodes as the excitation source.

2.3 Bioimaging

Fibroblasts L929 cells were cultured in a RPMI 1640 medium with 10% fetal bovine serum (FBS) at 37 ˚C in a 5% CO_2 atmosphere. The cells were cultured exponentially as a monolayer with a 70%–80% confluence. After reaching the optimum growth level, they were detached using trypsin-EDTA (1X). All the cell culture experiments were performed under sterile conditions. The cells were seeded on 24-well chambered cover glasses at a density of 1×10^6 cells/mL for 24 h. The GQDs, at varying concentrations, were added to the cell culture medium (500 μL). After incubating for 4 h, excess GQDs were removed by gently rinsing the medium three times with a phosphate buffered saline (PBS, pH 7.4) solution. The fluorescence images were collected by sequential line scanning with an Olympus FV1000 confocal laser-scanning microscope. The GQDs were excited at 420 nm and the resultant emission was collected in the range of 507–559 nm.

2.4 Cell viability assay

Cell viability was evaluated by the colorimetric 3-(4,5-dimethylthiazol-2-yl)-2,5 diphenyltetrazolium bromide (MTT) assay after treatment with the GQDs. 10,000 L929 cells were seeded onto 96-well tissue culture plates in sterile conditions. They were then incubated for 24 h in the absence or presence of GQD aqueous solutions (0.1, 0.5, 1, 3 and 5 μg/mL). The treated cells were then incubated for 4 h in the presence of the MTT solution prepared by dissolving 3-(4,5-dimethylthiazol-2-yl)-2,5 diphenyltetrazolium bromide in PBS (5 mg/mL). After incubation, the MTT solution was decanted and the formazan precipitate was dissolved in 1 mL dimethylsulfoxide (DMSO) at 37 ˚C. Only those cells with a functional mitochondria are capable of cleaving MTT to generate the dark purple formazan. The UV absorbance of the solubilized formazan crystals was measured spectrophotometrically at 490 nm. The cell viability was determined by the following equation, in which A stands for the amount of formazan determined for cells treated under different conditions, TC for treated cells, B for background, and UC indicates untreated cells.

$$\text{Viability}\,(\%)=\left[\left(A_{490\text{TC}}-A_{490\text{B}}\right)\Big/\left(A_{490\text{UC}}-A_{490\text{B}}\right)\right]\times 100 \quad (1)$$

3 Results and discussion

Figure 1(a) shows the optical image of the freeze-dried GQD powder derived from hollow CNOs. The GQD powder has a light-brown color, similar to that of graphene oxide. Figure 1(b) shows the appearance of the GQD aqueous solution under visible light and UV light. It was found that the aqueous solution of GQDs synthesized by the oxidation reaction of CNOs was clear with no sediment at the bottom of the cuvette. On the other hand, the GQDs produced from graphite flake precursors exhibit large black flakes after the reaction [20]. The large structure of graphite usually requires stronger oxidative agents, such as $KMnO_4$ along with the H_3PO_4 and H_2SO_4 used for synthesizing graphene oxide. Meanwhile, the high surface curvature and small crystalline domains of the CNO nanoparticles lead to much easier dispersion, exfoliation, functionalization and chemical cutting. The GQD aqueous solution under visible light is light brown in color and no precipitates were formed in the solution even after standing for several weeks at room temperature (23–28 ˚C). When illuminated with a UV wavelength of 320 nm, the GQD aqueous solution emits a yellow-green hybrid fluorescence, which can be attributed to the quantum confinement and surface functional groups. As shown in Fig. 1(c), the light passed in a straight path through the GQD aqueous solution under laser pointer emitting, which demonstrates the intrinsic Tyndall effect and colloidal characteristics of the GQDs. In Fig. 1(d), it can be seen that the GQD aqueous solution became muddy and that the sediment gradually settled at the bottom after adding 0.5 mL ethanol (99.9%). Ethanol is an unfavorable solvent for dissolving GQDs, and can be used to separate and purify them [28]. Figures 1(e) and 1(f) show the differences in the hydrophilic behavior of the hollow CNOs and the FeNi@CNOs. The hollow CNO aqueous dispersion exhibits little change in its color after sonicating (0.5 h), aging (5 h) and centrifuging, thus indicating the good hydrophilicity of the hollow CNOs. In contrast, the dramatic color change in the FeNi@CNOs aqueous dispersion after centrifuging implies that the FeNi@CNOs are much more hydrophobic.

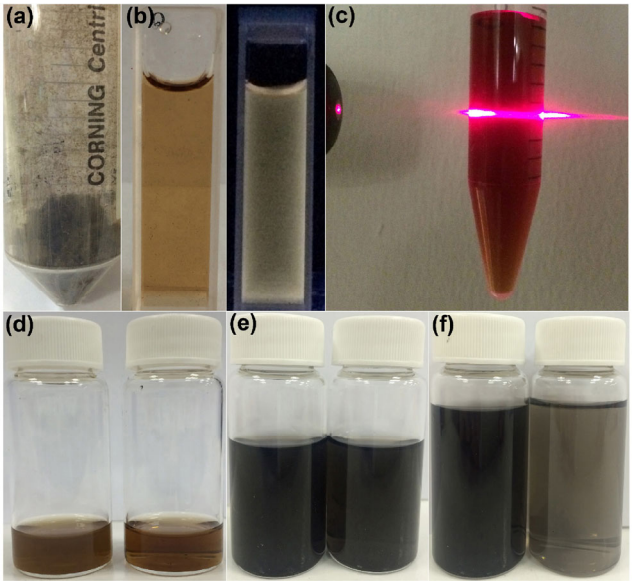

Figure 1 Optical images of the GQD solution and the CNO solutions. (a) Freeze-dried GQD powder, (b) the GQD aqueous solution under visible light and UV light of 320 nm wavelength, (c) Tyndall effect of the GQDs, as demonstrated by the straight path of the light through the GQD solution, (d) GQD aqueous solution before (right) and after (left) adding 0.5 mL ethanol (99.9%), (e) the hollow CNOs aqueous dispersion before (left) and after (right) centrifuging at 8,000 rpm for 10 min, and (f) the FeNi@CNOs aqueous dispersion before (right) and after (left) centrifuging at 8,000 rpm for 10 min.

Figures 2(a) and 2(b) show the TEM images of the hollow CNOs synthesized by our high temperature annealing process and those commercially procured, respectively. Both products show an inner hollow structure. Figure S1 in the Electronic Supplementary Material (ESM) shows that the high temperature annealing-derived hollow CNOs have a larger size (averaging at 20 nm) and thicker graphitic shells than the purchased CNOs. The TEM image of metal-encapsulating CNOs is displayed in Fig. 2(c). The TEM images of the products obtained from acid oxidation of the three precursors are shown in Figs. 2(d)–2(f). It can be seen that both types of the hollow CNOs yield GQDs with similar size distributions, whereas the FeNi alloy encapsulating CNOs yield only amorphous hollow structures (70–80 nm in size) with an irregular morphology. Other types of metal encapsulating CNOs (Fe@CNOs and Ni@CNOs) yield incompletely reacted hollow carbon onions (shown in Fig. S2 in the ESM). The volume expansion can be attributed to the gas formation during the acid oxidation reaction of carbon [29]. The metal-encapsulating CNOs were

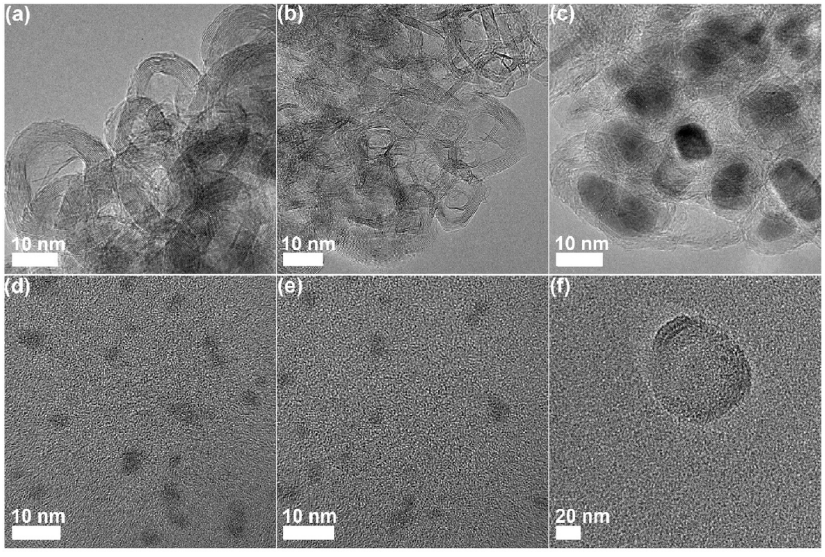

Figure 2 (a)–(c) TEM images of high-temperature annealing derived hollow CNOs, commercially derived hollow CNOs, and metal-encapsulating CNOs, (d)–(f) TEM images of the products obtained from the acid oxidation of the precursors in (a)–(c).

completely consumed during the reaction with no sedimentation in the flask. The resulting aqueous solution is brown in color under visible light, as can be seen in Fig. S3 in the ESM. However, these systems cannot be termed GQDs, according to their morphology.

The HRTEM images in Figs. 3(a) and 3(b) show the GQDs synthesized from high-temperature annealed hollow CNOs (HCNOs-derived GQDs) and commercial hollow CNOs (cHCNOs-derived GQDs), respectively. The crystalline hexagonal structures of the GQDs can be clearly seen, which are also demonstrated by the corresponding hexagonal lattices in the inset two-dimensional (2D) fast Fourier transform (FFT) images. The lattice fringe spacing of 0.20 nm shown in Fig. 3(a)

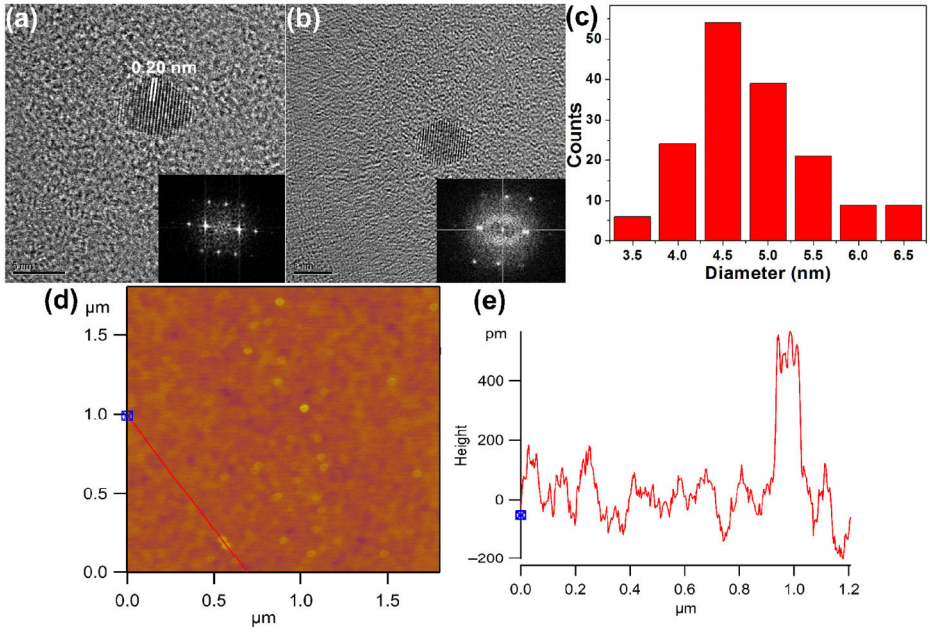

Figure 3 HRTEM images of the (a) HCNOs-derived GQDs and (b) cHCNOs-derived CNOs. The inset images in (a) and (b) are their corresponding FFT diffraction patterns. (c) The size distribution statistics of the cHCNOs-derived CNOs. (d) The AFM image and the section profile of the GQDs on the surface of the SiO_2 wafer. The blue cross-bar labels in (d) and (e) represent the start-point of the line drawing and height measurement baseline point, respectively.

corresponds to the (100) in-plane lattice of graphene. The size-distribution statistics in Fig. 3(c) show that the cHCNOs-derived GQDs have a narrow size distribution ranging from 3.5 to 6.5 nm, with an average lateral size of approximately 4.8 nm. According to the reports available in the literature, based on the density functional theory calculations, the bandgap in GQDs is around 0.5 eV [30]. Through extensive TEM observations (Fig. S4 in the ESM), we inferred that some graphene quantum dots consist of graphene cores and outer amorphous edge regions. This is consistent with the results reported earlier [20, 31]. The AFM image of the GQDs is shown in Fig. 3(d). It can be seen that the GQDs were uniform in size and were homogeneously dispersed on the surface of the SiO_2 wafer. The section measurement (Fig. 3(e)) shows that two typical GQDs have an average height of ~ 0.63 nm, which implies that the GQDs have a single graphene layer enriched with oxygen-containing functional groups on the surface.

High-resolution XPS measurements (Fig. 4(a)) were carried out to investigate the surface characteristics of the cHCNOs-derived CNOs. The peak assignments in the XPS spectra are as follows: graphitic sp^2 carbon at 284.5 eV, alcoholic carbon (C–O) at 286 eV, and carboxyl carbon (O–C=O) at 289 eV. The presence of these oxygen-containing bonds indicated that the surface of the GQDs were functionalized with hydroxyl, carbonyl, and carboxylic acid groups. The FTIR spectra in Fig. 4(b) further demonstrated that the GQD surface was decorated with abundant oxygenated functional groups, including hydroxyl (3,420 cm^{-1}), carboxyl (1,733 cm^{-1}), carbonyl (1,620 cm^{-1}), the epoxy (1,180 cm^{-1}) groups. The absorption at 1,380 cm^{-1} can be ascribed to the presence of the C–O bonds. These functional groups provide the GQDs with good water solubility. The hollow CNOs and the metal-encapsulating CNOs both show an appreciable number of carbonyl functional groups. However, compared to the hollow CNOs, the metal-encapsulating CNOs have lesser numbers of C–O bonds and epoxy groups, which makes them less hydrophilic. Raman characterization was carried out to investigate the variation in the sp^2-carbon after the oxidation of hollow CNOs. The relative intensity of the D-band to the G-band (I_D/I_G) in the GQDs is 0.95, which is higher than that of the hollow CNOs and results reported elsewhere [19, 20]. The greater number of defects resulted from the surface oxidation of the hollow CNOs. However, the minimally increased I_D/I_G ratio suggests that the sp^2-domain of the GQDs was well maintained. Compared to the hollow CNOs, the 2D band of the GQDs disappeared, indicating that the graphene domains in the CNOs have been deconstructed.

Figure 5(a) shows the UV–vis absorption spectra and fluorescence spectra of the GQDs aqueous solution. The absorbance peak at around 230 nm corresponds to the π–π^* transitions of the C=C bonds in the aromatic rings. This indicates the presence of a large π-electron system. The π-electron system can strongly couple with the surface electronic states created by the oxidation of the surfaces, and consequently alter the overall electronic structure of the GQDs [5]. The fluorescence spectra show that the GQDs emit at a fluorescence wavelength of 519 nm independent of the excitation wavelengths up to 480 nm, which is longer than previously reported [3, 13, 15]. This

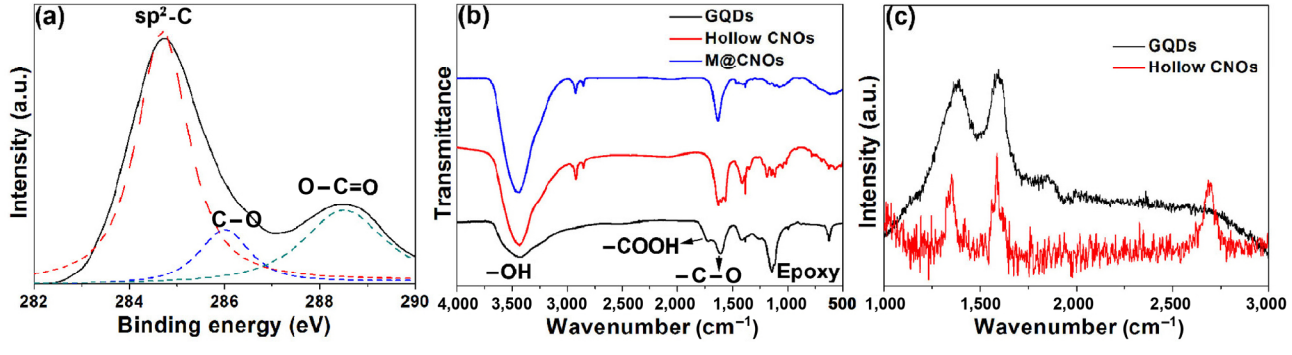

Figure 4 (a) XPS spectra of the GQDs, (b) FTIR and (c) Raman spectra of the GQDs and CNOs.

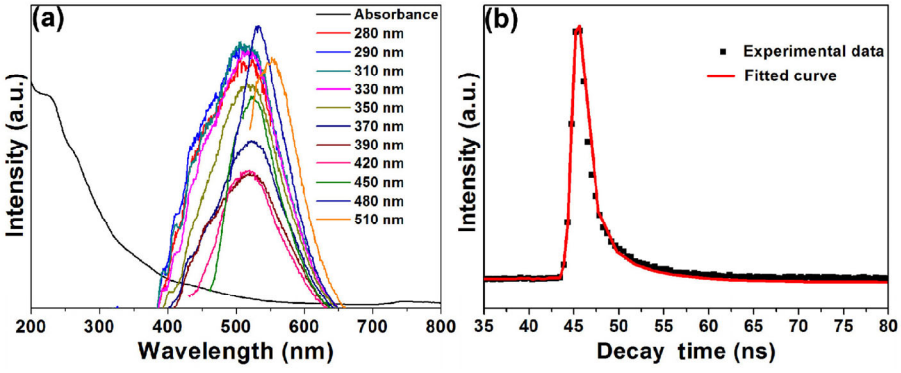

Figure 5 (a) UV–vis absorption and fluorescence spectra of the GQDs, and (b) time-resolved photoluminescence spectra of the GQDs along with the fitting curve.

suggests that the surface trap sites or the energy gap which cause the PL λ_{ex}-dependency are identical in the GQD species [1]. The long λ_{PL} and λ_{ex}, as well as the λ_{ex}-independent PL behavior even in the long λ_{ex} region are not harmful to the human body. This is also beneficial for biological or sensing applications where the fluorescence can be monitored under visible light excitation with no need for UV excitation. These results confirm the uniformity of our samples, in terms of their optical features. The above data, including the Raman, FTIR, and XPS results, clearly exhibit that our GQDs consist of π-conjugated domains in their carbon cores and amorphous regions on their surfaces. It has been reported that surface defects can serve as capture centers for excitons and thus give rise to surface-state-related fluorescence [5]. The carboxyl groups on the sp^2-hybridized carbons can also induce significant local distortions, resulting in a narrower energy gap [32]. The luminescence decay profile of the GQDs is shown in Fig. 5(b). The decay profile was recorded for the transitions of the GQDs at 519 nm for green emission under excitation at 370 nm; it was measured at room temperature by using a time-correlated single photon counting technique. The decay curve can be well fitted to a second-order exponential decay curve, as shown in Fig. 5(b). The lifetime of the GQDs was determined to be 1.22 μs according to the equation in the supporting information. The result shows that the lifetimes are short enough for potential solid-state lighting applications.

We have also synthesized GQDs with an average lateral size of 6 nm by reducing the oxidation reaction period to 3 h. Figure S5 in the ESM shows a red-shift on the main PL peak from 535 to 573 nm when the excitation wavelength increased from 330 to 480 nm. The different λ_{ex}-dependent PL behavior can be attributed to the quantum confinement in the differently-sized GQDs. The bandgap transitions in the GQDs are due to the conjugated sp^2-domains, and the sp^2-domain size dictates the quantum confinement effect [6]. From the TEM observations, the sp^2-domain size of the GQDs derived from the hollow CNO precursors is close to the average particle size of 4.8 nm, and comparable to that of the orange-emissive carbon nano-dots [6]. Unlike the blue- and ultraviolet-emissive GQDs obtained from CNOs [19], the larger conjugated sp^2-domain size and narrower size distribution of the hollow CNOs derived GQDs are responsible for the yellow-green hybrid luminescence and the λ_{ex}-independent PL behavior even at a long λ_{ex} of 480 nm. This means that the hollow CNO precursors are beneficial for producing GQDs with large sp^2-domains and a uniform size distribution. The inefficiency of the metal-encapsulating CNOs for synthesizing GQDs can be ascribed to two aspects: On one hand, the CNOs with encapsulated metals have less defects and are less hydrophilic than the hollow CNOs (as demonstrated in Figs. 1(f) and 4(b)). The M@CNOs cannot be dispersed properly in the acid solution, which results in a smaller surface area exposure and lower reaction speed. On the other hand, the acid can easily penetrate into the inner space of the hollow CNOs through their surface defects. The simultaneous reactions with the inner and outer graphene surfaces lead to rapid formation of carbon fragments and species. In contrast, the inner graphene

shell surface attached to the metal surface has a highly ordered sp^2-structure than that of the outer surface. Therefore, the inner graphene shells will not be easily oxidized into graphene fragments. Furthermore, the metal cations formed by dissolving metal particles in the acid solution will functionalize and passivate the graphene surface [6], thus slowing down the oxidation reaction.

Based on their fluorescence quenching properties, GQDs have been used as efficient probes for detecting heavy metal ions. In this regard, the GQDs can be used as an environmental toxicity indicator and a metal ion sensor in water treatment. Due to the λ_{ex}-independent PL behavior of our GQDs in the visible light region, we used visible light of 390 nm wavelength as the excitation source. Several heavy metal ions, including Co^{2+}, Cr^{3+}, Cu^{2+}, Mn^{4+}, Ni^{2+} and Zn^{2+}, were used for analyzing the selectivity of the GQDs. It can be seen from Fig. 6 that the fluorescence intensities of the GQD aqueous solutions were gradually suppressed upon increasing the concentration of the metal ions. Of all the tested ions, only Cu^{2+} at a concentration of 600 μM, can fully quench the fluorescence of the GQDs. In contrast, the fluorescence peak of the GQD aqueous solution showed no obvious change after adding Zn^{2+}. Furthermore, Cu^{2+} is the most sensitive ions species among the ions tested for the fluorescence quenching of the GQD aqueous solution. At a concentration of 20 μM, the Cu^{2+} ions show the lowest F/F_0 value (F and F_0 are the fluorescence intensities of the probes at 519 nm in the presence and absence of the metal ions, respectively) of 0.23, demonstrating the high selectivity of the GQDs for detecting Cu^{2+} among the different types of metal ions. The F/F_0 values of Co^{2+}, Cr^{3+}, Mn^{2+}, Ni^{2+} and Zn^{2+} at concentration of 20 μM were 0.51, 0.30, 0.71, 0.64 and 0.98, respectively. The lowest F/F_0 of Cu^{2+} is in agreement with the previous reports [10, 11]. The F/F_0 value of the Cu^{2+} (2 μM) in GQD aqueous solution was 0.73, which is comparable to the detection limit reported earlier [10]. The quantitative relationship between the F/F_0 value and the Cu^{2+} concentration is shown in Fig. S6 in the ESM. A nonlinear relationship is observed, indicating that the fluorescence quenching is not induced by collision. To demonstrate the feasibility of the detection of Cu^{2+} by GQDs with longer excitation wavelengths in the absence of UV excitation, the fluorescence quenching by Cu^{2+} ions at different concentrations was analyzed at excitation wavelengths of 450 and 480 nm. It can be seen in Fig. S7 in the ESM that the fluorescence intensities

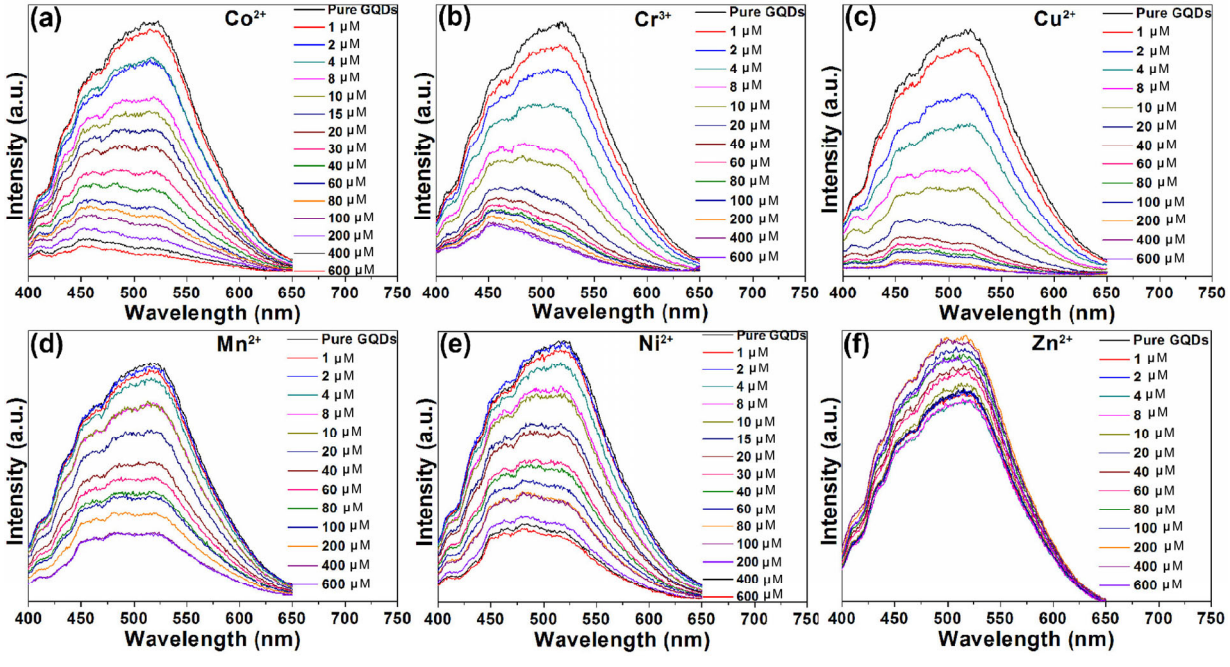

Figure 6 The fluorescence spectra of GQDs quenched by different metal ions at different concentrations (a) Co^{2+}, (b) Cr^{3+}, (c) Cu^{2+}, (d) Mn^{2+}, (e) Ni^{2+} and (f) Zn^{2+}.

can still be fully quenched by the Cu^{2+} ions at their highest concentration at 450 and 480 nm excitation. The quantitative relationship between F/F_0 and Cu^{2+} concentration shown in Fig. S7(c) in the ESM suggests that the sensing ability of the GQDs at excitation wavelengths of 450 and 480 nm is similar.

Both GQDs and carbon nanodots [12] have been reported to show potential application in cell imaging. The current cHCNOs-derived GQDs can be potentially used as non-toxic bioimaging probes operating under visible light excitation in applications such as cell tracking or protein analysis. L929 cells were chosen to evaluate the *in vitro* cellular imaging behavior of the GQDs. Figure 7 shows the images of the cells incubated for 4 h in the GQD aqueous solution (concentration up to 100 μg/mL). It can be seen in Fig. 7(b) that the cells can be visualized with a fluorescent color at an excitation wavelengths of 420 nm. The fluorescence was predominant in the cell peripheral, and weak in the cell nucleus. As can be seen in the bright field image (Fig. 7(a)), the cells show no blinking or photobleaching, indicating the high photo-stability and biocompatibility of the GQDs. The fluorescence intensity of the cellular imaging was not high, indicating that the GQDs translocated into the L929 cells via a low energy passive transport process [3]. We also carried out the cell imaging under excitation at a longer wavelength of 488 nm. As can be seen in Fig. S8 in the ESM, the L929 cells can be clearly visualized in the dark field. This demonstrates that the GQDs can be used as cell bioimaging probes under excitation at long wavelengths up to 488 nm, which provides a safe way for cell tracking. The cytotoxicity of the GQDs on the L929 cells was also evaluated by assessing cell viability by the MTT assay. As can be seen in the cell viability profile (Fig. S9 in the ESM), in the GQD concentration range of 0.1 to 5 μg/mL, the cell viability values were higher than 90%. At concentrations higher than 0.1 μg/mL, ~ 10% increase in the cell viability could be seen. Furthermore, there is no toxicity observed in the tested concentration range from 0.5 to 5 μg/mL. This demonstrates that the GQDs have a minimal cytotoxic effect on the L929 cells.

4 Conclusions

We have demonstrated that hollow CNOs precursors are beneficial for synthesizing GQDs with a yellow-green hybrid luminescence and a λ_{ex}-independent PL behavior. This behavior persisted in the λ_{ex} range of 280 to 480 nm. In contrast, metal encapsulation in the CNO precursor structures was disadvantageous for synthesizing GQDs due to their less hydrophilic graphene surfaces and slow rate of acid oxidation. The GQDs derived from the hollow CNO precursors can potentially be used in sensing and cell imaging applications, with longer excitation wavelengths in the visible light region. Under visible light excitation up to 480 nm, efficient hollow CNO derived GQD sensing probes for detecting Cu^{2+} ions have been demonstrated. This means that environmental sensing and bioimaging can be accomplished in the ambient environment with no need for UV excitation. Our work provides a reference for obtaining the desired PL behavior by tailoring the CNO precursor structures in terms of their inner space.

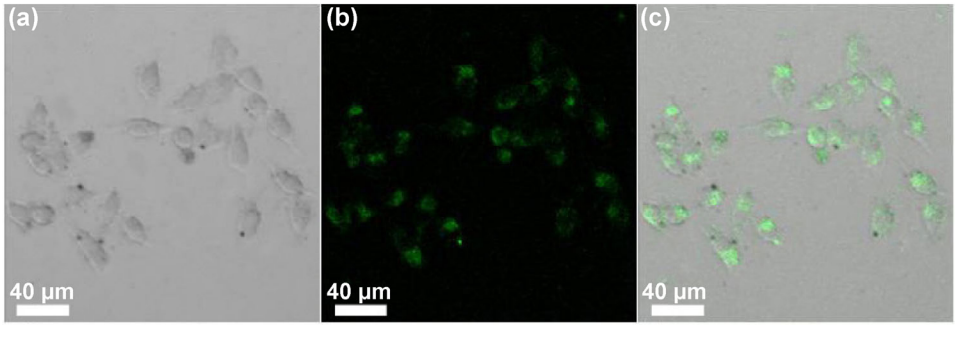

Figure 7 Confocal microscopy images of the L929 cells under excitation at 420 nm. (a) Bright field image, (b) fluorescence image, and (c) merge image of the GQD incubated cells.

Acknowledgements

The authors acknowledge the finance support by the Natural Science Foundation of Tianjin City (No. 16JCYBJC41000) and support by Tianjin Key Subject for Materials Physics and Chemistry.

Electronic Supplementary Material: Supplementary material (synthesis process of CNOs, equations for calculating lifetime of GQDs, more TEM and digital photograph imaging, PL spectra, and confocal microscopy images) is available in the online version of this article at https://doi.org/ 10.1007/s12274-017-1617-0.

References

[1] Baker, S. N.; Baker, G. A. Luminescent carbon nanodots: Emergent nanolights. *Angew. Chem., Int. Ed.* **2010**, *49*, 6726–6744.

[2] Zhu, S. J.; Song, Y. B.; Zhao, X. H.; Shao, J. R.; Zhang, J. H.; Yang, B. The photoluminescence mechanism in carbon dots (graphene quantum dots, carbon nanodots, and polymer dots): Current state and future perspective. *Nano Res.* **2015**, *8*, 355–381.

[3] Zheng, M.; Ruan, S. B.; Liu, S.; Sun, T. T.; Qu, D.; Zhao, H. F.; Xie, Z. G.; Gao, H. L.; Jing, X. B.; Sun, Z. C. Self-targeting fluorescent carbon dots for diagnosis of brain cancer cells. *ACS Nano* **2015**, *9*, 11455–11461.

[4] Park, Y.; Yoo, J.; Lim, B.; Kwon, W.; Rhee, S. W. Improving the functionality of carbon nanodots: Doping and surface functionalization. *J. Mater. Chem. A* **2016**, *4*, 11582–11603.

[5] Bao, L.; Liu, C.; Zhang, Z. L.; Pang, D. W. Photoluminescence-tunable carbon nanodots: Surface-state energy-gap tuning. *Adv. Mater.* **2015**, *27*, 1663–1667.

[6] Sun, Q. N.; Zhou, D.; Li, D.; Ji, W. Y.; Jing, P. T.; Han, D.; Liu, L.; Zeng, H. B.; Shen, D. Z. Toward efficient orange emissive carbon nanodots through conjugated sp^2-domain controlling and surface charges engineering. *Adv. Mater.* **2016**, *28*, 3516–3521.

[7] Jiang, K.; Sun, S.; Zhang, L.; Lu, Y.; Wu, A. G.; Cai, C. Z.; Lin, H. W. Red, green, and blue luminescence by carbon dots: Full-color emission tuning and multicolor cellular imaging. *Angew. Chem., Int. Ed.* **2015**, *54*, 5360–5363.

[8] Tetsuka, H.; Nagoya, A.; Fukusumi, T.; Matsui, T. Molecularly designed, nitrogen-functionalized graphene quantum dots for optoelectronic devices. *Adv. Mater.* **2016**, *28*, 4632–4638.

[9] Buzaglo, M.; Shtein, M.; Regev, O. Graphene quantum dots produced by microfluidization. *Chem. Mater.* **2016**, *28*, 21–24.

[10] Hu, C.; Yu, C.; Li, M. Y.; Wang, X.; Yang, J. Y.; Zhao, Z. B.; Eychmüller, A.; Sun, Y. P.; Qiu, J. S. Chemically tailoring coal to fluorescent carbon dots with tuned size and their capacity for Cu(II) detection. *Small* **2014**, *10*, 4926–4933.

[11] Liu, Y. Y.; Kim, D. Y. Ultraviolet and blue emitting graphene quantum dots synthesized from carbon nano-onions and their comparison for metal ion sensing. *Chem. Comm.* **2015**, *51*, 4176–4179.

[12] Wang, Z. G.; Fu, B. S.; Zou, S. W.; Duan, B.; Chang, C. Y.; Yang, B.; Zhou, X.; Zhang, L. Facile construction of carbon dots via acid catalytic hydrothermal method and their application for target imaging of cancer cells. *Nano Res.* **2016**, *9*, 214–223.

[13] Li, Y.; Zhao, Y.; Cheng, H. H.; Hu, Y.; Shi, G. Q.; Dai, L. M.; Qu, L. T. Nitrogen-doped graphene quantum dots with oxygen-rich functional groups. *J. Am. Chem. Soc.* **2012**, *134*, 15–18.

[14] Zhao, Q. L.; Zhang, Z. L.; Huang, B. H.; Peng, J.; Zhang, M.; Pang, D. W. Facile preparation of low cytotoxicity fluorescent carbon nanocrystals by electrooxidation of graphite. *Chem. Commun.* **2008**, 5516–5518.

[15] Arcudi, F.; Đorđević, L.; Prato, M. Synthesis, separation, and characterization of small and highly fluorescent nitrogen-doped carbon nanodots. *Angew. Chem., Int. Ed.* **2016**, *55*, 2107–2112.

[16] Sun, Y. P.; Zhou, B.; Lin, Y.; Wang, W.; Fernando, K. A. S.; Pathak, P.; Meziani, M. J.; Harruff, B. A.; Wang, X.; Wang, H. F. et al. Quantum-sized carbon dots for bright and colorful photoluminescence. *J. Am. Chem. Soc.* **2006**, *128*, 7756–7757.

[17] Hu, S. L.; Trin chi, A.; Atkin, P.; Cole, I. Tunable photoluminescence across the entire visible spectrum from carbon dots excited by white light. *Angew. Chem., Int. Ed.* **2015**, *54*, 2970–2974.

[18] Dong, Y. Q.; Chen, C. Q.; Zheng, X. T.; Gao, L. L.; Cui, Z. M.; Yang, H. B.; Guo, C. X.; Chi, Y. W.; Li, C. M. One-step and high yield simultaneous preparation of single- and multi-layer graphene quantum dots from CX-72 carbon black. *J. Mater. Chem.* **2012**, *22*, 8764–8766.

[19] Peng, J.; Gao, W.; Gupta, B. K.; Liu, Z.; Romero-Aburto, R.; Ge, L. H.; Song, L.; Alemany, L. B.; Zhan, X. B.; Gao, G. H. et al. Graphene quantum dots derived from carbon fibers. *Nano Lett.* **2012**, *12*, 844–849.

[20] Ye, R. Q.; Xiang, C. S.; Lin, J.; Peng, Z. W.; Huang, K. W.; Yan, Z.; Cook, N. P.; Samuel, E. L. G.; Hwang, C. C.; Ruan, G. D. et al. Coal as an abundant source of graphene quantum dots. *Nat. Commun.* **2013**, *4*, 2943.

[21] Shenderova, O.; Grishko, V.; Cunningham, G.; Moseenkov, S.; McGuire, G.; Kuznestov, V. Onion-like carbon for terahertz electromagnetic shielding. *Diam. Relat. Mater.* **2008**, *17*, 462–466.

[22] Lu, J.; Yeo, P. S. E.; Gan, C. K.; Wu, P.; Loh, K. P. Transforming C_{60} molecules into graphene quantum dots. *Nat. Nanotechnol.* **2011**, *6*, 247–252.

[23] Li, Y.; Hu, Y.; Zhao, Y.; Shi, G. Q.; Deng, L. E.; Hou, Y. B.; Qu, L. T. An electrochemical avenue to green-luminescent graphene quantum dots as potential electron-acceptors for photovoltaics. *Adv. Mater.* **2011**, *23*, 776–780.

[24] Park, B.; Kim, S. J.; Sohn, J. S.; Nam, M. S.; Kang, S.; Jun, S. C. Surface plasmon enhancement of photoluminescence in photo-chemically synthesized graphene quantum dot and Au nanosphere. *Nano Res.* **2016**, *9*, 1866–1875.

[25] Zhang, C. G.; Li, J. J.; Liu, E. Z.; He, C. N.; Shi, C. S.; Du, X. W.; Hauge, R. H.; Zhao, N. Q. Synthesis of hollow carbon nano-onions and their use for electrochemical hydrogen storage. *Carbon* **2012**, *50*, 3513–3521.

[26] Zhang, C. G.; Li, J. J.; Shi, C. S.; He, C. N.; Liu, E. Z.; Zhao, N. Q. Self-anchored catalysts for substrate-free synthesis of metal-encapsulated carbon nano-onions and study of their magnetic properties. *Nano Res.* **2016**, *9*, 1159–1172.

[27] Zhang, C. G.; Li, J. J.; Shi, C. S.; He, C. N.; Liu, E. Z.; Zhao, N. Q. Effect of Ni, Fe and Fe-Ni alloy catalysts on the synthesis of metal contained carbon nano-onions and studies of their electrochemical hydrogen storage properties. *J. Energy Chem.* **2014**, *23*, 324–330.

[28] Deng, L.; Wang, X. L.; Kuang, Y.; Wang, C.; Luo, L.; Wang, F.; Sun, X. M. Development of hydrophilicity gradient ultracentrifugation method for photoluminescence investigation of separated non-sedimental carbon dots. *Nano Res.* **2015**, *8*, 2810–2821.

[29] Shang, J. J.; Xie, B. B.; Li, Y.; Wei, X.; Du, N.; Li, H. P.; Hou, W. G.; Zhang, R. J. Inflating strategy to form ultrathin hollow MnO_2 nanoballoons. *ACS Nano* **2016**, *10*, 5916–5921.

[30] Son, Y. W.; Cohen, M. L.; Louie, S. G. Energy gaps in graphene nanoribbons. *Phys. Rev. Lett.* **2006**, *97*, 216803.

[31] Ding, H.; Yu, S. B.; Wei, J. S.; Xiong, H. M. Full-color light-emitting carbon dots with a surface-state-controlled luminescence mechanism. *ACS Nano* **2016**, *10*, 484–491.

[32] Chien, C. T.; Li, S. S.; Lai, W. J.; Yeh, Y. C.; Chen, H. A.; Chen, I. S.; Chen, L. C.; Chen, K. H.; Nemoto, T.; Isoda, S. et al. Tunable photoluminescence from graphene oxide. *Angew. Chem., Int. Ed.* **2012**, *51*, 6662–6666.